

A shorter version of this paper was submitted to the IRRMA-V Meeting  
(Bologna, ITALY; 9-14 June 2002)

**Modelling Topic:**

**Monte Carlo methods of radiation transport, applications to design**

**COMPARISON AND PHYSICAL INTERPRETATION OF MCNP AND TART  
NEUTRON AND GAMMA MONTE CARLO SHIELDING CALCULATIONS  
FOR A HEAVY-ION ICF SYSTEM**

**E. Mainardi** (University of Rome "La Sapienza", C.so Vittorio Emanuele II,  
244 – 00186 Rome, Italy – E-mail: [enrico@nuc.berkeley.edu](mailto:enrico@nuc.berkeley.edu)),

**F. Premuda** (University of Bologna, Italy), **E. Lee** (LBNL, Berkeley, USA)

**Abstract**

For heavy-ion beam driven inertial fusion "liquid-protected" reactor designs such as HYLIFE-II, a mixture of molten salts made of  $F^{10}$ ,  $Li^6$ ,  $Li^7$  and  $Be^9$  (called flibe) allows small chambers and final-focus magnets closer to the target with superconducting coils suffering higher radiation damage, though they can stand only a certain amount of energy deposited before quenching. This work has been primarily focusing on verifying that total energy deposited by fusion neutrons and induced gamma rays remain under such limit values and the final purpose is the optimization of the shielding of the magnetic lens system from the points of view of the geometrical configuration and of the physical nature of the materials adopted.

The system is analyzed in terms of six geometrical models going from simplified up to much more realistic representations of a system of 192 beam lines, each focused by six magnets.

A 3-D transport calculation of the radiation penetrating through ducts, that takes into account the complexity of the system, requires Monte Carlo methods. The quantities analyzed, using the two codes MCNP and TART include: neutron mean free path and total path length dependence on energy, energy deposited by neutrons and gamma photons, values of the total fluence integrated in the whole energy range, and the neutron spectrum in different zones of the system.

The technical nature of the design problem and the methodology followed were presented in a previous paper by summarizing briefly the results for the deposited energy distribution on the six focal magnets. Now a much more extensive comparison of the performances of the two codes for different configurations of the system is discussed, separating the n and  $\gamma$  contributions, in the light of the physical interpretation of the results in terms of first flight and of scattered neutron fluxes, of primary  $\gamma$  and of secondary  $\gamma$  generated by inelastically scattered or radiatively captured neutrons. The final conclusions indicate some guidelines and suggest possible improvements for the future neutronic design of a heavy ion beam fusion facility named IRE (Integrated Research Experiment) to be realized in the USA.

*PACS:* 52.58.H, 28.52, 02.50.U, 29.85.+c, 02.70Lq, 41.75.L

*Keywords:* Heavy-ion inertial fusion energy, Heavy-ion final focus system, Models for Monte Carlo neutronic calculations, Energy deposited by neutrons and photons, Shielding for neutrons and photons.

## Introduction

Inertial Confinement Fusion (ICF) aims to induce implosions of deuterium and tritium pellets to obtain an extremely dense and hot plasma, then transforming the energy generated by fusion in heat transferred by the coolants surrounding the target to a heat exchanger. Turbine generators finally transform thermal energy into electricity.

While lasers are now used to induce D-T pellet implosions, the future power plants could use heavy-ion beams instead. This approach is considered to have advantages in efficiencies and repetition rate.

Over the last two decades, researchers in the Lawrence Livermore National Laboratory and the Lawrence Berkeley National Laboratory, University of California at Berkeley, and several other locations, have developed a number of innovative Inertial Fusion Energy (IFE) target-chamber and reactors designs for both laser and heavy-ion driven targets.

For heavy-ion fusion, recent research has focused on “liquid-protected” designs that allow highly compact target chambers. In the design of a reactor such as HYLIFE-II [1, 2], the liquid used is a molten salt made of  $F^{10}$ ,  $Li^6$ ,  $Li^7$ ,  $Be^9$  (called flibe) that:

1. is a coolant that transfers the energy deposited by neutrons and photons to the heat exchanger;
2. generates new tritium via lithium-neutrons interactions;
3. reduces the number and energy of neutrons reaching the chamber walls and devices next to it;
4. protects the chamber wall from x-rays and debris.

Thus flibe allows the final-focus magnets to be closer to the target, which helps to reduce the focus spot size and in turn the size of the driver, with a large reduction of the cost of IFE electricity.

Consequently the superconducting coils of the magnets closer to the D-T neutron source will potentially suffer higher damage though they can stand only a certain amount of energy deposited before quenching. The aim of our calculations is to determine the energy deposited by fusion neutrons and induced gamma rays in the superconducting magnetic lenses focusing the heavy-ion beams. Such a neutronic study of a final focus system, with six magnets in each beam line duct, requires a 3D transport calculation of neutron and gamma fluxes accompanied by an accurate analysis of the physical meaning of the numerical results in a complex geometrical configuration, accounting for the needs dictated by different technical, engineering, and physical areas of design. In fact the reactor HYLIFE-II consists of 192 beam lines to provide access to the heavy ions that implode the pellet. So there are a total of 1152 final focus magnets close to the chamber.

A 3-D transport calculation of the radiation penetrating through ducts with bends and/or steps, that takes into account the complexity of the system, requires a Monte Carlo simulation applied to appropriate models representing geometry and material composition. The parameters are optimized using an accurate analysis of six geometrical models developed starting from the simplest, with results very dependent on geometry and shielding materials.

The calculations of the Monte Carlo code named TART 98 [3], developed at Lawrence Livermore National Laboratory (LLNL) are compared with those obtained by the Monte Carlo code MCNP4B [4], developed at Los Alamos National Laboratory (LANL). The results obtained with the two codes turned out to be in good agreement with each other within their Standard Deviation (STD). This work refers to [5] and [6] with additional details for the comparison of the two codes and for the physical analysis. The source restriction angle bias technique (explained in details in [5] and [6]) gives reliable results as it is proved comparing re-normalized results with those for a  $4\pi$  source. Hence this technique is used in all the six models, avoiding other variance reduction techniques, to have reasonable computing time, and meaningful and sufficiently accurate results.

Here attention is essentially centered on the physical separate analysis of the neutronic and photonic shielding results that will suggest solutions for optimizing the system from the neutronic point of view, with respect to both relative position of the magnets and choice of shielding materials.

Even small variations in the radial position of superconducting magnets can influence strongly the fraction of first flight neutrons reaching a magnet coming directly with high energy from the fusion source and consequently the damage to the magnets and also the gamma photon sources induced in the magnets together with the related shielding needs; the presence in the magnet of the gamma photon sources induced by neutrons requires also an investigation of the shielding material properties for  $\gamma$  emission and attenuation in view of the optimal design choices.

Hence neutron fluxes and energy deposited are to be evaluated and analyzed in order to separate the effects of scattered from those of first flight neutrons, to account separately for the energy deposited directly by neutrons and for the direct gamma doses plus those induced by neutron inelastic scattering and radiative captures and so learn how minimize the effect of first flight neutrons and of secondary gamma rays.

Another important effect analyzed here is the neutronic interaction between the neighboring ion beam lines, that strongly increases the energy deposited with respect to the values computed for a single beam line. This study indicates that in view of limiting this effect appropriate radial shielding materials are needed: optimal choices of the isotopic components are selected.

The goals of the work are to gain experience and to identify possible practical information starting from simplified models in order to use them in more complex and realistic models. A scheme of the method used is described in Figure 1.

The answers for the different zones of such a system include:

1.  $E_{NP}$ =values of energy deposited by Neutrons (N) and Photons (P). In (MeV/n, J/cc)
  2.  $\phi_{INT}$  =values of the total fluence integrated in all energy range. In ( $1/cm^2$ )
  3.  $\phi(E)$  =neutron spectrum in energy. In ( $1/cm^2$ )
  4.  $L(E)$  =total path length of Neutrons (N) in energy. In (cm)
  5.  $\lambda(E)$  =neutron mean free path in energy in the materials. In (cm)
- $E_{LIM}=1mJ/cc$  =prescribed limit to prevent quench of superconducting coils

## **2. Two simplified models of a final focus duct for TART/MCNP comparison: source angle bias verification, physical analysis of shielding materials and geometrical effects on neutron and gamma photon transport**

The models presented here, that are a simplification of a final focus penetration in an IFE chamber as regard geometry and materials adopted, are appropriate comparing the two codes TART and MCNP in a benchmark problem: to verify the accuracy of the source angle restriction technique (angle-bias with renormalization of the results to reduce the computational times in view of the successive treatment of more complex models of the system) and to test the sensitivity of the results to the change of the cross section libraries adopted; even more interesting were their use for investigating aspects of the physical behavior of the materials. Finally the comparison between the results for the two simplified models is important in identifying the influence of a step, present in the first and not in second (Figure 2a, 2b), and so of the geometrical configuration of the system.

The first simplified 3-D model (*angle*) is shown in Figure 2a. The 14.1 MeV neutron source is located at the origin of a cone of a major penetration in the chamber. The geometry includes a “step” due to the presence of a second cone between 12m and 15m with origin at 9m. In the case called *angle* the source is restricted to emit neutrons over the solid angle subtended by the half-amplitude  $\alpha = \text{ATAN}(100/900) = 6.34^\circ$ , while in the case called *fix* the neutrons are emitted over  $4\pi$ . To re-normalize, the results are to be multiplied by  $f=2\pi(1-\cos\alpha)/4\pi=3.06 \cdot 10^{-3}$ .

In the second simplified 3-D model (*cone* in Figure 2b) there is not a second cone and so no step between zones 4 and 6, the source being still restricted to  $\alpha = 6.34^\circ$ .

In both geometrical models a cylinder, that contains in zones 3 and 5 the coils of the first magnet, is present outside the cones; zones 3 and 5 are filled with iron, other zones are filled with air (in place of vacuum).

According to Table 1 the results for  $E_{np}$  obtained restricting the source to  $\alpha$  and re-normalizing are in very good agreement with the cases of neutrons emitted over  $4\pi$  and are affected by smaller standard deviations (STD).

Although the comparison between the energy deposited separately by neutrons and photons computed by TART and MCNP (see e.g. Table 2) shows some discrepancies -especially in zones 3 and 5-, the values of the cumulative energy deposited by neutrons + photons, evaluated by TART and MCNP (Table 3), are in good agreement apart from zone 3.

The energy deposited by photons in zones with matter at solid density is an order of magnitude greater than that deposited by neutrons, i.e. neutronic inelastic scattering and radiative capture yield  $\gamma$ 's to be shielded unless special isotopic components are adopted in shields.

Table 4 shows that the results are insensitive to different nuclear data libraries.

While the peak of highest energy of Figure 3 is obviously due to the 14.1 MeV energy of the source neutrons, the peaks at lower energies correspond to "windows" in energy for neutrons.

The effects of the step present in the first model (angle) and not in the second (cone) appear in Figure 3 and Table 5: in the case "angle" the zone 5, more exposed to first flight neutrons, collects an energy deposited higher by an order of magnitude than that collected in the case "cone"; further the greater amount of first flight neutrons arriving at zone 5 is confirmed by the peaks in neutron spectrum present in zone 5 for the case "angle" and absent in the same zone in the case "cone", when it is better shielded by zone 3.

In zone 3 the energy deposited is less for the case "angle" than in the case "cone" due to the greater energy deposited in zone 5 by the collided neutrons coming back to interact with zone 3 having less remaining energy. Obviously the actual possibility of axial shielding effective in order to attenuate first flight neutron flux is the interposition of flibe between the source and magnets immediately after each fusion event, combined to fixed shielding zones before the magnets outside the cone of the first flight neutrons. However, the oscillating flibe jets cannot close the conic hole, created for heavy-ions access to the chamber, in the available time (of the order of 1.0  $\mu$ sec).

### **3. The influence of the radial distance on the energy deposited on the coils of the first magnet protected by flibe according to the third model.**

Figure 4 shows the third model geometry, which includes the first magnet, without adjacent shields, the flibe jets liquid and first wall. A source of 14.1 MeV neutrons at the origin emits neutrons in a cone of half-aperture  $\gamma = 0.52^\circ$ . In next

model, zones 11 and 12, now filled by air, shall contain shields. **Flibe**, a mixture of molten salts isotopically constituted as in Table 6, is intermediate to 2 spheres at 0.30m and 1.0m from the origin. The first wall, made of **SS304** steel, is intermediate to 2 spheres at 3.5m and 4.5m from the origin and exhibits a conic hole. The **first magnet** is located 5.20m from the origin and is 1.0m long. Figure 5 shows  $Enp(c)$  in the zones 9 of magnet coils, made of NbTi, cooled with liquid Helium and represented as the homogeneous mixture of Table 7, and collar zone 10. According to the more conservative standards the coils can stand values  $Enp \leq Elim = 1mJ/cc$ .

The graphic representation of  $Enp(c)$  by Figure 5 can be used to determine the optimal position for the coils considering that:

- 1) For  $c < 7.25$  cm the magnet is inside the cone of first flight neutrons;
- 2)  $Elim = 1m J/cc$  and  $c < 13$  cm allows many beam lines;
- 3) For  $c = 4.83$  cm first flight neutrons (FFN) with collided ones and induced  $\gamma$ 's lead to  $Enp > Elim$ ;
- 4) For  $c > 7.25$  the absence of FFN yields  $Enp < Elim$  and for rising  $c$  H field intensity, magnet volume and costs increase.

The consideration of STD so leads to choose  $c = 9$  cm. as optimal. Lower values of  $Enp$  with increasing values of  $c$  are due to the leakage out of the system of collided neutrons that terminate their history without coming back in the structure. The different behavior from  $c=13cm$  to  $c=14.49cm$  might depend on the higher STD for higher  $c$ .

The effect of neutron interaction from neighbouring beam lines will bring in more collided neutrons, causing more difficulty to keep  $Enp$  and  $\phi_{INT}$  below maximum values to guarantee margins against quench.

#### **4. The effect of different materials on neutrons and gamma radial and axial shields on the energy deposited and fluences for the first magnet**

The same geometry, source, angle bias parameters and running conditions of section 3 are used here in our fourth model to see the effect of different shielding materials, placed in radial (zone 11) and axial (zone 12) positions, to protect the coils of the first magnet of one beam line. These materials can be or a mixture of 98% iron, 2% borated water (case **m**) described in Table 8, or polyethylene  $(CH_2)_n$  (case **p**) or air (case **a**).

Although the coils radial position of  $c=9cm$  guarantees  $Enp < 1mJ/cc$  for one beam line even if no shield is assumed (case **a**), nevertheless shielding will be needed for the  $Enp$  is increased due to collided neutrons coming from other beam lines. The expected results from the interpolation of Figure 5 of course agree with the results for  $Enp$  in A case of Table 9.

As expected Table 9 shows that the material *m* turns out to be much better than material *p* in reducing energy deposition in the coils as *m* slows down neutrons of high energy by inelastic scattering in iron (impossible for *p*) while water slows down epithermal neutrons by elastic scattering with hydrogen, preparing neutrons to be absorbed in boron by radiative capture. According to Table 9 most energy is deposited in zones 11 and 12 by photons as fast neutrons dissipate a lot of their energy in shields through  $\gamma$  production consequent to neutron inelastic scattering with iron and to radiative captures in boron. The generated  $\gamma$ 's can interact, dissipating their energy, with the quite dense cloud of electrons of iron. Since  $B^{10}$  does not emit  $\gamma$ 's by radiative ( $n, \gamma$ ) capture when absorbing neutrons, but only emits  $\alpha$ 's, an increase in its isotopic abundance in *m* could decrease energy deposited by photons. On the contrary with the material *p* photon energy deposited ( $E_p$ ) in shields (zones 11 and 12) is very low, being *p* not able to slow down fast neutrons by inelastic scattering, but only slow neutrons by elastic interactions.

A comparison TART/MCNP is presented by Table 10. A reason for the discrepancies could be the different sets of nuclear data adopted.

### **5. The contribution of neutrons collided in 8 neighbouring beam lines to the energy deposition in a central one.**

The geometry of this fifth model includes the eight beam lines that surrounds a penetration in a IFE chamber (Figures 6a, 6b). The purpose of considering the first superconducting magnet in each of the nine beam lines is to see the effect of collided neutrons coming from adjacent beam lines. The source of 14.1 MeV neutrons is located at the origin of nine cones with half-aperture  $\gamma = 0.52^\circ$ , with source restricted to  $\alpha = \text{ATAN} [45 \cdot \text{RADQ}(2)/520] = 6.98^\circ$  to include all 9 beam line cones (Figures 6a, 6b). The number of neutrons generated per fusion shot is  $1.48 \cdot 10^{20}$  n concentrate in the interesting directions by the angle bias technique.

The radial position of the coils of the first magnet is assumed to be  $c=9$  cm that guarantees  $E_{np} < 1$  m J/cc for just one beam line without shielding. Now  $E_{np}$  assumes a value about double as it is possible to see in Table 11 if compared with Table 9, due to the presence of collided neutrons coming from eight beam lines adjacent to a main central one, though flibe jets, first wall and shielding materials be those previously considered.

The material *m* is used in this model not only for radial and axial shields but also as infra-magnets shielding with purpose to protect the magnets from collided neutrons coming from adjacent beam lines. If  $E_{lim}=1\text{mJ/cc}$  is adopted as an upper limit for  $E_{np}$  in the coils, an optimization of shielding performance in composition and thickness is needed. The use of larger quantities of iron and the increase of the isotopic

abundance of  $\text{Fe}^{57}$  and  $\text{B}^{10}$  would probably bring  $\text{Enp}$  below  $\text{Elim}$ . Bigger values of the coil radial distance  $c$  would probably decrease  $\text{Enp}$  but higher magnetic field will be required to have the same focusing effect on the ion beams, implying higher costs due to higher volumes of materials. Also a different  $\text{Elim}$  value of 20mJ/cc has been suggested; in this case all the magnets would have  $\text{Enp}$  well below this limit.

## **6. Radial, axial, infra-magnets shields for all six superconducting magnets in one beam line**

Figure 7 shows a single beam line with all the six magnets included in sixth model and Tabs 11a and 11b give its dimensions. As a first approximation all the six magnets are considered with the same magnet geometry (cylinders with radial and axial shields) and same shielding material (98% iron, 2% borated water).

The radial position of the coils of the first magnet is assumed to be  $c=9\text{cm}$ , which guarantees  $\text{Enp}<1\text{mJ/cc}$  for just one beam line without shielding. For the other five magnets other  $c$  values (Table 16b) are assumed as a first guess considering the ion beam maximum dimension and the section of neutron cone. The radial parameters can be optimized considering the results of Table 12.

The  $\text{Enp}$  in the coils (zone 9) of the first magnet seems to be low enough, but with many adjacent beam lines,  $\text{Enp}$  in the superconducting coils is doubled to overcome the prescribed limits if the performance of shields is not improved.

The  $\text{Enp}$  in the coils (zone 19) of the second magnet according to Table 12 is below the value computed for previous zone due to larger distances both longitudinally from the source and radially from the center axis of the beam line. Thus the problems for this magnet discussed in [5] are not neutron shielding.

The shielding of the third and fourth magnet should be already appropriate as the  $\text{Enp}$  in the coils (zones 29 and 39) are below the limit value  $\text{Elim} = 1\text{mJ/cc}$  also doubling the values of Table 12 according to Chap. 5 of [6] to take into account the contribution of collided neutrons and  $\gamma$ 's from the adjacent beam lines. The increase of  $\text{Enp}$  from zone 9 and 19 to zones 29 and 39 might be due to the bigger radial distance of zone 19 from neutron line of sight. Also is possible that collided neutrons and gamma rays from the first two magnets are directed towards the third magnet.

For the fifth and sixth magnet an alternative shielding strategy should be found, since the  $\text{Enp}$  values in the coils (zones 49 and 59) are above  $\text{Elim}= 1\text{mJ/cc}$  even for one beam line only. Though the coils are outside the neutron line of sight, part of the radial shield is inside the source cone and so is intersected by first flight neutrons, generating collided neutrons and inducing gamma rays directed from radial shielding toward the coils. This effect when added to the  $\text{Enp}$  due to neutrons and gamma rays coming from other directions could partially explain the bigger  $\text{Enp}$  values in zones 49

and 59. Collided neutrons and gamma rays coming from previous magnets increase the values for  $En_p$  on a particular magnet; so a deeper investigation of this phenomenon can bring to an optimization of the magnet reciprocal positions from the neutronics point of view in compatibility with electromagnetic and other structural issues. Also other HIF studies like HIBALL-II found such an oscillating behavior of  $En_p$  and fluence values for magnets along the beam line.

## 7. Conclusions

The considerations developed on  $En_p$ 's in the conditions of Table 12 constitute a basis for further studies of the problem.

Apart from the reasons discussed in [5] for a redesign of the second magnet, the other issues to be investigated refer to the oscillating values of  $En_p$  overcoming in the last two magnets the maximum  $Elim$  fixed to avoid too short time of quenching.

These issues are related to specific shielding problems and to the effects of material distribution on the neutron and gamma transport, taking into account the joined constraints of the many beam line cones, of the axial and radial positions with respect to the first flight neutron cone and of the reciprocal positions of the magnets together with their magnetic characteristics and dimensions; the reciprocal positions of the magnets can strongly influence the amount of the energy deposited in a magnet by neutrons collided in the other magnets and by gamma photons induced in these magnets by neutron inelastic scattering and radiative absorption. A clear indication of the above discussed is the relevance of the energy deposited by  $\gamma$ 's and so the need of minimizing the emission  $\gamma$ 's from radiative captures inside a specific magnet and its shield, where  $En_p$  is evaluated, but also in different magnets of the same line or even in the adjacent beam lines. As neutron radiative capture in coils cannot be avoided, it is important to reduce the phenomenon inside infra-magnet shields, radial and axial shields, choosing a material with the unique boron  $B^{10}$  isotope emitting only  $\alpha$  particles and no  $\gamma$ 's when absorbing a neutron. The efficiency of neutron slowing down by inelastic scattering is also to be maximized by the choice of  $Fe^{57}$  isotope in material  $m = \text{iron} + \text{borated water}$ . Once verified the influence of such isotopic abundances could be remarkable; the increase of the shielding material costs could be compensated by the advantage of decreasing the energy deposited inside the coils, placed of course together with related shields outside the first flight neutron cones, without imposing any change in the geometry of the magnetic lens system. It is better for a magnet to have no radial shield rather than a radial shield inside the first flight neutron cone producing collided neutrons and gamma rays induced by inelastic scattering contributing to increase energy deposited in the magnet coils that the radial shield should protect.

## **Acknowledgements**

The authors acknowledge the important suggestions for an optimal use of the code TART by Dr. Cullen and Dr. Latkowski of the *Lawrence Livermore National Laboratory* (LLNL). The help of Dr. Burn and Dr. Gualdrini (ENEA-Bologna), Dr. Harding (LLNL), Jerome Verbeke, Darren Bleuel (LBNL) has been very valuable for the MCNP part. Thanks also to Professor Vujic, Peterson and Greenspan of the department of Nuclear Engineering of the *University of California at Berkeley* (UCB). E. Mainardi wishes to thank the Heavy Ion Fusion Group of the *Lawrence Berkeley National Laboratory* (LBNL) for the kind hospitality, encouragements and funds during his stay at LBNL. This work was also partially funded by a Grant of the Engineering School of Bologna for Thesis Research abroad.

## **References**

- [1] R.W. Moir et al., HYLIFE-II: a molten-salt inertial fusion energy power plant design – Final Report, *Fusion Technol.* 25 (1984) 5.
- [2] R.W. Moir et al., HYLIFE-II Progress Report, UCID-21816, 4.82-100.
- [3] D.E. Cullen, TART97: A Coupled Neutron-Photon 3-D Combinational Geometry Monte Carlo Transport Code, Lawrence Livermore National Laboratory, UCRL-ID-126455, Rev. 1, November, 1997.
- [4] Briesmeister (Ed.), MCNP – A General Monte Carlo N-Particle Transport Code, Version 4B, La-12625-m, March 1997, Los Alamos National Laboratory.
- [5] E. Mainardi, F. Premuda, E. Lee, Neutronic calculations for a final focus system, *Nucl. Inst. Meth. Phys. Res. A*, vol. 464/1-3 (2001), pp. 410-415.
- [6] E. Mainardi (F. Premuda, E. Lee advisors), Monte Carlo neutronic calculations for the final focus magnets of an IFE facility, Master Thesis in Nuclear Engineering, University of Bologna, July 1999.

### Figure captions

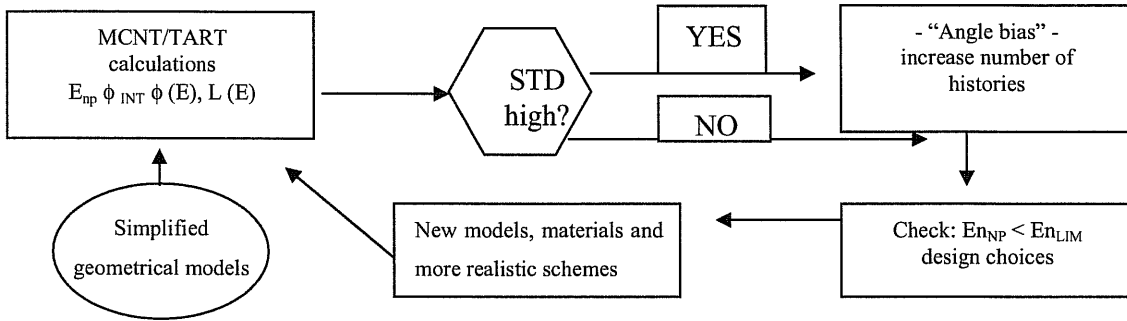


Figure 1: Scheme of the computational method.

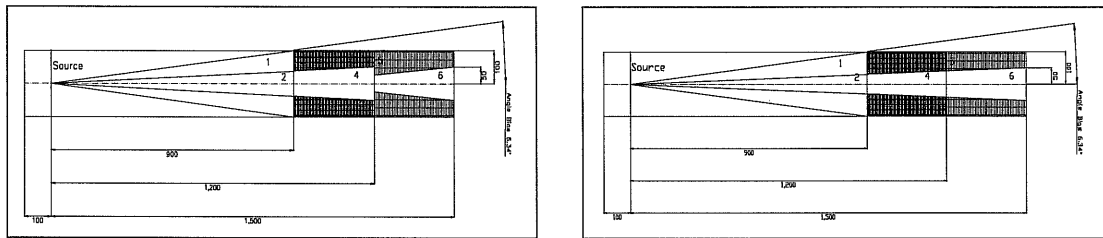


Figure 2a,b: 2-D longitudinal view, obtained with AUTOCAD-14, with the numbers of the zones and dimensions in cm for the first and second simplified models (Angle and Cone Models).

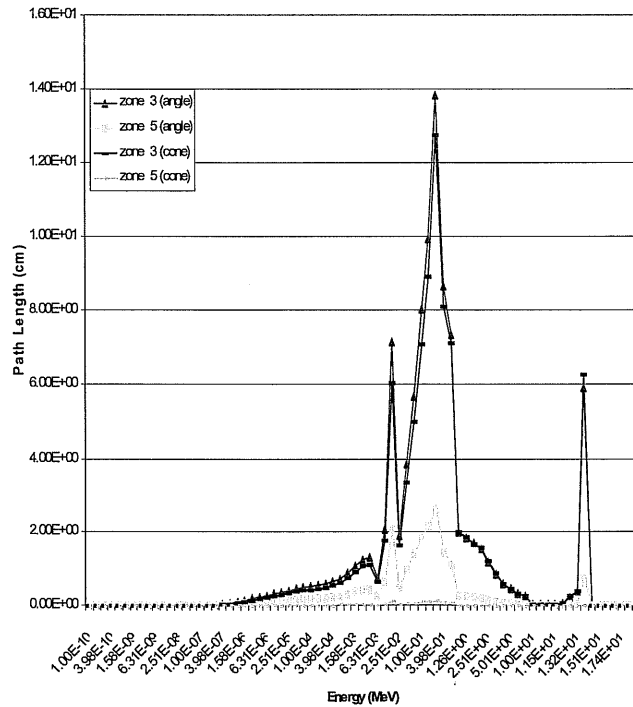


Figure 3: Total neutron path length as a function of energy for Model 1 (angle) and Model 2 (cone) in comparison.

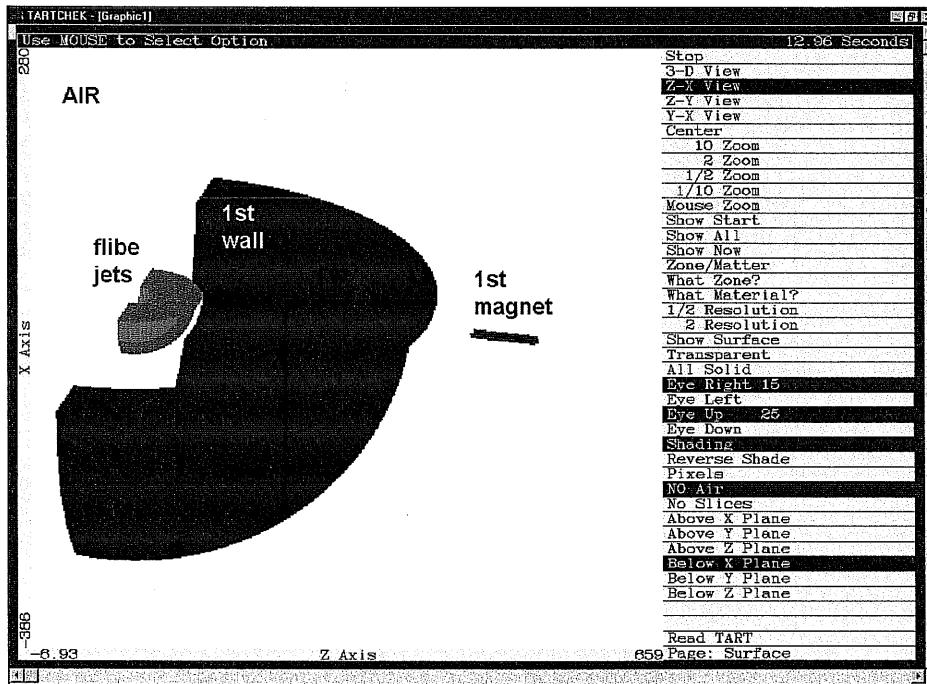


Figure 4: 3D-view of the system (source + flibe + first wall + magnet) obtained by TARTCHEK.

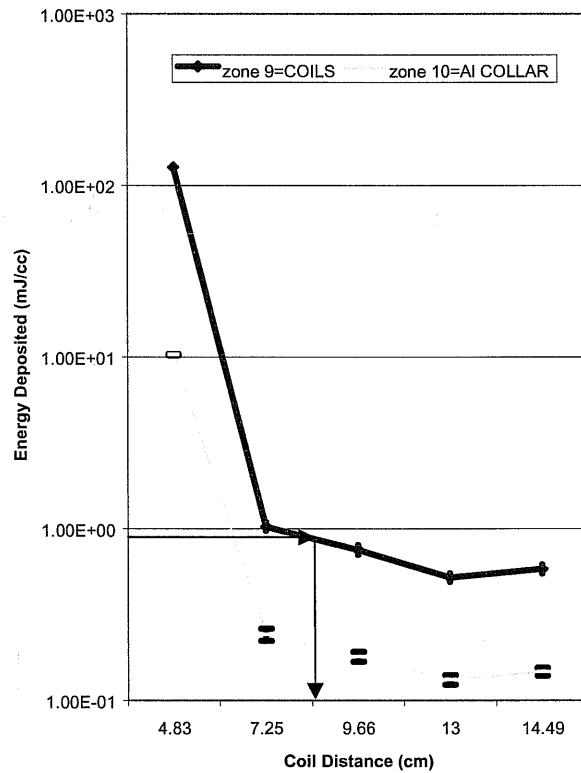


Figure 5: Energy deposited totally (N+P) in zones 9, 10 as a function of radial distance  $c$ .

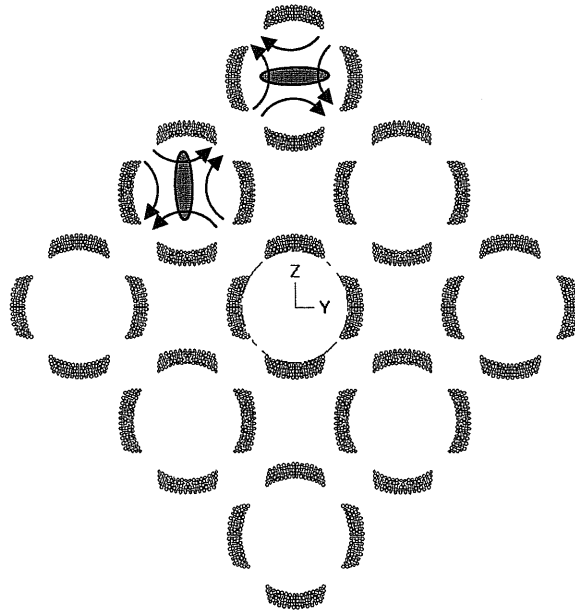


Figure 6a: 2D frontal view of the array of 9 beam lines of heavy ions obtained from Dr. Rainer Meinke.

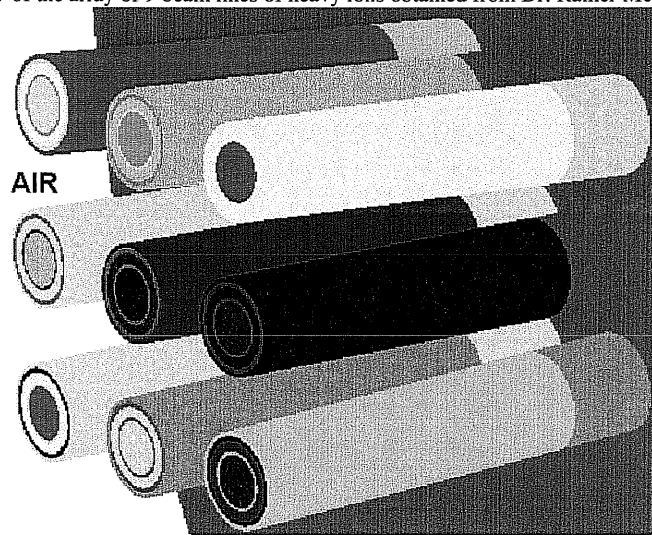


Figure 6b: 3D-view of the system of many focalized ion beams obtained by TARTCHEK.

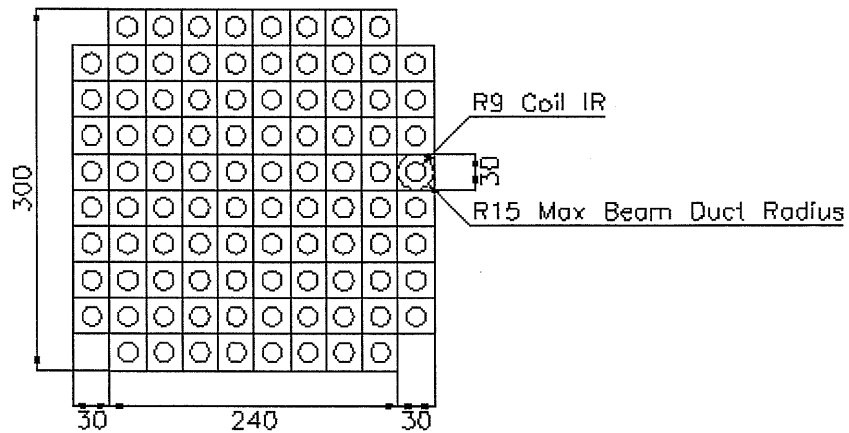


Figure 6c: 2D frontal view of the array of 96 beam lines of heavy ions (total of 192 for both sides).

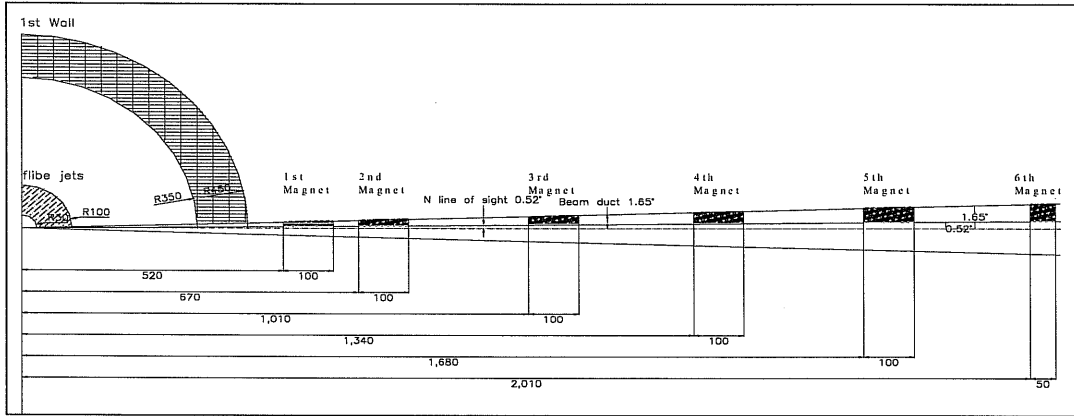


Figure 7a: Longitudinal 2-D view of the upper half of a beam line with six magnets (Model 6).

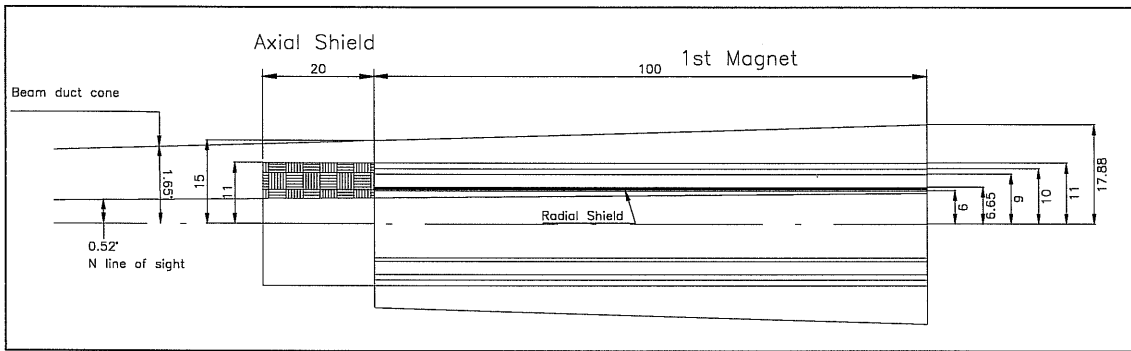


Figure 7b: Longitudinal 2-D view of the upper half of the first magnet.

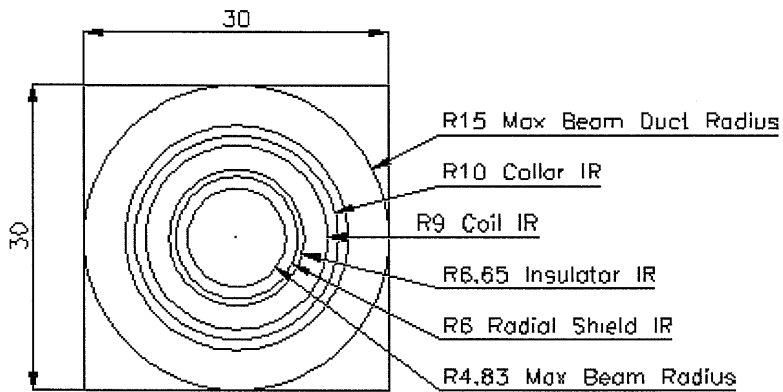


Figure 7c: Radial 2-D view of the first magnet.